International Journal of Pharmaceutics 623 (2022) 121895

Contents lists available at ScienceDirect

International Journal of Pharmaceutics

journal homepage: www.elsevier.com/locate/ijpharm

Nanoclay-reinforced HA/alginate scaffolds as cell carriers and SDF-1 delivery-platforms for bone tissue engineering

Itsasne Erezuma [a,b], Izeia Lukin [a,b], Carolina Pimenta-Lopes [c], Francesc Ventura [c], Patricia Garcia-Garcia [d,e], Ricardo Reyes [e,f], Mª Rosa Arnau [g], Araceli Delgado [d,e], Nayere Taebnia [h,i], Firoz Babu Kadumudi [j], Alireza Dolatshahi-Pirouz [j], Gorka Orive [a,b,k,*]

[a] NanoBioCel Research Group, School of Pharmacy, University of the Basque Country (UPV/EHU), Vitoria-Gasteiz, Spain
[b] Bioaraba, NanoBioCel Research Group, Vitoria-Gasteiz, Spain
[c] Departament de Ciències Fisiològiques, Universitat de Barcelona, IDIBELL, L'Hospitalet de Llobregat, Spain
[d] Department of Chemical Engineering and Pharmaceutical Technology. Universidad de La Laguna, 38200 La Laguna, Spain
[e] Institute of Biomedical Technologies (ITB), Center for Biomedical Research of the Canary Islands (CIBICAN), Universidad de La Laguna, 38200 La Laguna, Spain
[f] Department of Biochemistry, Microbiology, Cell Biology and Genetics, Universidad de La Laguna, 38200 La Laguna, Spain
[g] Servicio del Estabulario, Universidad de La Laguna, 38200 La Laguna, Spain
[h] Department of Physiology and Pharmacology, Karolinska Institutet, SE-171 77 Stockholm, Sweden
[i] Center for Intestinal Absorption and Transport of Biopharmaceuticals, Department of Health Technology, Technical University of Denmark, 2800 Kgs. Lyngby, Denmark
[j] Department of Health Technology, Technical University of Denmark, 2800 Kgs. Lyngby, Denmark
[k] Biomedical Research Networking Centre in Bioengineering, Biomaterials and Nanomedicine (CIBER-BBN). Vitoria-Gasteiz, Spain

ARTICLE INFO

Keywords:
3D Scaffold
Bone
Biomaterials
Nanoclay
Tissue Engineering
SDF-1

ABSTRACT

Bone tissue engineering has come on the scene to overcome the difficulties of the current treatment strategies. By combining biomaterials, active agents and growth factors, cells and nanomaterials, tissue engineering makes it possible to create new structures that enhance bone regeneration. Herein, hyaluronic acid and alginate were used to create biologically active hydrogels, and montmorillonite nanoclay was used to reinforce and stabilize them. The developed scaffolds were found to be biocompatible and osteogenic with mMSCs *in vitro*, especially those reinforced with the nanoclay, and allowed mineralization even in the absence of differentiation media. Moreover, an *in vivo* investigation was performed to establish the potential of the hydrogels to mend bone and act as cell-carriers and delivery platforms for SDF-1. Scaffolds embedded with SDF-1 exhibited the highest percentages of bone regeneration as well as of angiogenesis, which confirms the suitability of the scaffolds for bone. Although there are a number of obstacles to triumph over, these bioengineered structures showed potential as future bone regeneration treatments.

1. Introduction

Tissue engineering (TE) is an interdisciplinary field with the formidable aim of restoring or substituting damaged tissues. To that end, TE involves different areas such as biology, engineering, nanotechnology or material science, creating neo-tissues or organs that can improve the path of health-issues (Vacanti, et al., 2020). In the case of bone, current strategies lack the power to mend tissue-involving pathologies, since the ongoing treatments are insufficient to heal the tissue completely (Dimitriou, et al., 2011; Salgado, et al., 2004). TE can be an ideal approach to remedy these issues and provide medicine with new and advantageous materials and techniques (Salgado, et al., 2004; Vacanti, et al., 2020).

Among the different advantages, TE allows for the design and fabrication of bioengineered scaffolds that can be a suitable approach to restore bone (Vacanti, et al., 2020). A three-dimensional (3D) scaffold that works as a temporary matrix for bone growth, supplying the tissue with an adequate environment, architecture and possibly growth factors to induce cell proliferation and tissue regeneration (Amiryaghoubi, et al., 2020; Salgado, et al., 2004). Between the wide varieties of scaffolds, hydrogels have stood out for their exclusive properties. These structures consist of highly hydrated 3D polymeric networks with specific features that boost the regeneration: biocompatibility, biodegradability and the ability to mimic the native milieu (Bai, et al., 2018; Lee

* Corresponding author at: NanoBioCel Research Group, School of Pharmacy, University of the Basque Country (UPV/EHU), Vitoria-Gasteiz, Spain.
E-mail address: gorka.orive@ehu.es (G. Orive).

https://doi.org/10.1016/j.ijpharm.2022.121895
Received 21 March 2022; Received in revised form 24 May 2022; Accepted 3 June 2022
Available online 9 June 2022

and Mooney, 2001). Despite their favorable characteristics, conventional hydrogels are not biomechanically ideal (Zhang and Khademhosseini, 2017), which limits their application in bone tissue engineering.

In order to emend the aforementioned obstacle, nanomaterials has exhibited great potential to provide favorable properties facilitate regeneration with the use of novel. These materials interact covalently or physically with polymer chains, and provide strength and enhancing biological abilities (Deo, et al., 2015). Following this line, scientists have added 2D nanosilicates – also called nanoclays – to improve the hydrogels stiffness. Not only do those nanoparticles have the ability to improve mechanical properties, but they also induce osteogenesis, which directly affects the effectiveness of the manufactured systems (Gaharwar, et al., 2019). Furthermore, due to the electrostatic interactions between the nanoclays and other molecules, they have been employed to create combinatorial delivery-platforms (Erezuma, et al., 2021; Khatoon, et al., 2020; Ogay, et al., 2020).

Myriad of natural factors such as stromal cell-derived factor 1 (SDF-1), bone morphogenic protein (BMP), transforming growth factor β (TGF-β) or insulin-like growth factor type 1 (IGF-1) have been studied and used for bone tissue engineering purposes (Garg, et al., 2017). Among them, the employment of SDF-1 -also called C-X-C motif chemokine 12 (CXCL12) - has to be highlighted. This growth factor is associated with several activities in the human body, among which the recruitment and retention of progenitor cells on the injury site aligns well with the scope of the current study, namely bone regeneration (Gilbert, et al., 2019; Lau and Wang, 2011).

In this context, Hasany et al, published an extensive study on double cross-linked nanoclay-reinforced hydrogels (Hasany, et al., 2018). The authors combined hyaluronic acid (HA), alginate and 2D nanoclays – Laponite (LP), montmorillonite (MMT) and sumecton (SUM) - to create 63 different hydrogel formulations. Their promising results showed that some of these hydrogels – the ones with MMT– were able to carry and enhance osteogenic differentiation of human mesenchymal stem cells (hMSC) even in a differentiation-factor-free media. Furthermore, they demonstrated that those structures are more resilient, shear-thinning, load-bearing and shock absorbing in comparison to pristine hydrogels. When it comes to osteogenic properties, the MTT-incorporated hydrogels display excellent potential, as evident from the increased ALP enzyme activity and the formation of mineralized matrix with the same composition as *in vivo* (Hasany, et al., 2018). This study has the focus on scaffolds characterization, biomechanical properties and *in vitro* experiments, without leaving evidence of the *in vivo* performance of them.

The present work has the objective of further advancing the study of HA-Al (C2) and HA-Al-MMT (M2) hydrogels and evaluating their *in vitro* potential and *in vivo* efficiency. Furthermore, the ability of hydrogels to act as cell-carriers and releasing platforms for SDF-1 was tested. Our study has followed the path of the previous work (Hasany, et al., 2018), but adding new aspects that expand the potential application of these scaffolds in bone tissue engineering.

2. Materials & methods

2.1. Nanocomposite hydrogel fabrication

C2 and M2 hydrogels were formed using thiol-modified hyaluronic acid (HA, HyStem® Cell Culture Scaffold Kit, Sigma-Aldrich), 8-arm PEGacrylate (8PEGA, MW = 10 kDa, Creative PEGworks) and alginate (Al, pharmaceutical grade, FMC Biopolymer, U.K.), as described previously (Hasany, et al., 2018). In the case of M2, montmorillonite (MMT, BYK) was used as the reinforcing nanoclay.

Initially, stock solutions of each component were prepared before proceeding to the scaffolds fabrication according to the following concentrations: HA 1.1% (w/v), Al 4% (w/v), 8PEGA 9% (w/v) and MMT 2.3% (w/v). To start preparing the hydrogels first HA and Al were mixed (together with MMT in the case of M2 hydrogels). Then, 8PEGA solution was added and the mixture was gently pipetted together. Finally, the forming hydrogel was deposited on silicon molds to create round shaped systems. Afterwards, to activate the second crosslinking mechanism 2% (w/v) calcium chloride ($CaCl_2$) solution was added on the top of the hydrogels. When crosslinking was completed, all samples were cleansed with Dulbecco's Phosphate-Buffered Saline (DPBS, Sigma-Aldrich, Spain).

Final concentrations of each component can be found in Table 1.

2.2. Protein adsorption studies

Previously prepared and freeze-dried C2/M2 scaffolds were utilized for this study. Hydrogels were reconstituted in DPBS and weighted before starting the experiment. Then, hydrogels were dipped in a Bovine Serum Albumin (BSA, Sigma-Aldrich) solution (1 mg/ml) for 24 h at 37 °C under constant shaking. Later, scaffolds were washed multiple times with DPBS to remove all the unbound protein. To detach and measure BSA protein the scaffolds were then immersed/submerged in an SDS (Sigma-Aldrich) solution of 2% (v/v) overnight and the BSA concentration in each sample was quantified. MicroBCA™ (Thermo Scientific) assay was performed according to manufacturer's protocol and the results were displayed as μg BSA adsorbed per mg hydrogel.

2.3. Cell cultures

Murine bone marrow-derived mesenchymal stem cells (mMSCs, C57BL-6 J) were cultured in DMEM (30–2002, ATTC) supplemented with fetal bovine serum (FBS 10%) and penicillin/streptomycin (P/S 1%) obtained from Fisher Scientific, Spain. Mouse L-929 fibroblasts were cultured with EMEM (30-2003™, ATTC) enriched with FBS 10% and P/S 1%. In both cases cells were harvested and used upon reaching confluence.

2.4. Fabrication of cell-laden scaffolds

mMSCs were utilized at passage 10–15 for all cell viability, differentiation and mineralization studies. mMSC suspension was mixed with C2 or M2 solution before the addition of 8PEGA and therefore prior to forming the hydrogels. The cellular concentration per hydrogel was 5×10^6 cells/ml. In order to confirm that cells were homogeneously distributed within the scaffold, images were taken using TE2000-S microscope (Nikon).

Cell-laden hydrogels were cultured with normal media (Diff -) -DMEM (30–2002) supplemented with FBS 10% and P/S 1%- or differentiation media (Diff +) –DMEM (30–2002) enriched with FBS 10%, P/S 1%, dexamethasone (0.5 μM), ascorbic-acid (200 μM) and β-glycerophosphate (10 mM) obtained from Sigma-Aldrich, Spain.

2.5. Biocompatibility assay

Biocompatibility of the manufactured scaffolds was performed using mouse L-929 fibroblasts, as explained by Echave and co-workers (Echave, et al., 2019), which were performed according to ISO 10993 guideline (Biological evaluation of medical devices guideline: cytotoxicity on extracts and cytotoxicity by direct contact). The viability was measured in the case of both cell-scaffold direct and indirect interaction –contact with extracts. Metabolic activity of the cells was evaluated

Table 1
Scaffolds composition (%(w/v)).

Component	Concentration % (w/v)
HA	0.50
Al	0.35
8PEGA	0.80
MMT	0.29

trough CCK-8 assay and the absorbance was determined using Tecan Infinite M2000 microplate reader at 450 nm. To normalize the data, metabolic activity of the cells without any contact with scaffolds or their extracts was hold as 100% of viability.

2.6. Live/Dead viability assay

Cell-laden scaffolds were stained at days 1, 5, 7, and 14 using a Live/Dead evaluation kit (Life Technologies) guided by manufacturer's protocol. Live cells (stained with Calcein-AM) were seen as green, whilst dead cells (stained with ethidium homodimer-1) were seen as red. Fluorescence micrographs were taken using Nikon TMS confocal laser scanning microscope.

2.7. Alkaline phosphatase (ALP) activity

To evaluate the intracellular alkaline phosphatase (ALP) activity of the encapsulated cells at week 1, 2 and 3, BCIP/NBT (ThermoFisher, Spain) solution was employed. Before staining, cell-laden scaffolds were treated with 1.6 M sodium citrate for 12 h to cleave the ionic links between the alginate chains and make the scaffold clearer. Then, the scaffolds were washed three times with DPBS, and the samples were completely covered with the staining solution and incubated in a light-protected environment and at room temperature (RT) for 2 h. Afterward, scaffolds were again washed three times with DPBS. Stained scaffolds were observed under Nikon AZ100 microscope and optical images were taken. Image J software was used as a tool to analyze the images. The black-violet stained area was estimated applying a threshold. The entire area of the scaffold was considered as 100% and scaffolds at day 1 were utilized to normalize data.

2.8. Alizarin red S staining and quantification

Extracellular calcium deposition was stained and measured by Alizarin Red S (ARED) staining. Staining solution was prepared by dissolving 1 g of ARED powder (Sigma-Aldrich) in 50 mL of mili-Q water. To complete the staining solution, pH was fine-tuned to 4.2 ± 0.1 and the solution was filtered through a 0.45 μm filter.

Before staining, cells were fixed in 4% paraformaldehyde around 30 min. Later, scaffolds were washed with DPBS three times and completely immersed in the staining solution for 1 h at RT without light. Afterward, scaffolds were washed multiple times with DPBS and they were let overnight to remove un-bond ARED.

Images were taken using Nikon AZ100 microscope and bonded ARED was measured using HCl as extracting agent. Once all ARED was extracted, it was quantified at 490 nm with Tecan Infinite M2000, using a calibration curve. The values of each condition were normalized to the control hydrogels (samples at day 1).

2.9. Scanning electron microscopy (SEM) and energy dispersive X-ray spectroscopy (EDAX) analysis

To determine the apatite mineral formation within the scaffolds, SEM and EDAX were employed. The hydrogels were first washed, lyophilized (48 h), and cross-sectioned. Before SEM imaging, all samples were sputter-coated with gold (10 nm). Then, images were achieved with SEM (AFEG 250 Analytical ESEM (FEI Quanta FEG 250)) operating at an accelerating voltage of 5 kV to confirm mineralization.

The EDAX analysis was performed in advance to gold sputtering by utilizing an energy-dispersive X-ray spectrometer (EDX; Oxford Instruments 80 mm^2 X-Max silicon drift detector) connected to SEM instrument operating at an accelerating voltage of 15 kV. Elemental compositions of scaffolds were reported in weight percentage, and corresponding Ca/P ratio was estimated by dividing the calcium weight percentage by that of phosphorous.

2.10. Fourier transform infrared spectroscopy (FTIR) analysis

Scaffolds were washed multiple times and lyophilized prior to the assay. FTIR spectra was taken using a PerkinElmer Spectrum 100 FTIR spectrometer assembled with a diamond crystal attenuated total reflectance accessory after background subtraction. Transmittance spectra of lyophilized samples were collected over the range of 4000–500 cm^{-1} with 16 scans at a resolution of 4 cm^{-1}. PerkinElmer Spectrum software was employed to correct the background and normalize all the data. Four parts of each sample were measured, and the averaged spectra were calculated for the study.

2.11. X-ray powder diffraction (XRD) analysis

Samples were washed and lyophilized before analysis. XRD analysis was performed using a HUBER G670 X-ray powder diffractometer (Germany) using the image plate detection method in the Guinier geometry. Analysis was carried out in the 2θ range of 10−80° at a step size of 0.005°, and diffractometer was equipped with secondary monochrome and Cu X-ray tube. The sealed tube X-ray generator was operated at 40 kV and 40 mA to provide Cu Kα1 radiations of wavelength 1.54056 Å.

2.12. In vivo studies

The animal experiments were carried out in conformity with the European Directive (2010/63/UE) on Care and Use of Animals in Experimental Procedures. Furthermore, animal protocols were previously accepted by the Ethics Committee for Animal Care of the University of La Laguna (CEIBA2014-0128). The surgeries were performed under isoflurane anesthesia. Analgesia comprised buprenorphine (0,01 mg/kg) subcutaneously previous to surgical procedures and paracetamol (200 mg/kg) was administered in the drinking water, for 3 days post-surgery. Besides, posterior to surgical recovery, animals were conceded free movement, food and water. Four experimental groups were used for each type of scaffold (C2/M2): controls with empty lesion, blank scaffolds, scaffolds embedded with mMSCs and scaffolds with a final concentration of 50 ng/ml of SDF-1 (Abcam).

2.12.1. Animal surgery

Animals were subjected to a surgery to produce a defect on calvaria bone tissue and subsequently, scaffolds with different treatments were implanted. In brief, calvaria bone was exposed and a 4 mm circular area was created using a biopsy punch. Then, a 4 mm circular transosseous defect was produced with a trephine bur (Rodríguez-Évora, et al., 2013). The scaffolds were introduced in the defects and skin of every animal was stapled. 8 weeks after implantation animals were sacrificed by CO_2 inhalation and defect area was extirpated.

2.12.2. Histology, histomorphometry and immunohistochemistry

In order to find out scaffolds ability to regenerate previously created critical size defect, extracted samples were prepared for histological analysis as previously reported (Hernández, et al., 2012). Shortly, samples were fixed with 4% paraformaldehyde solution, decalcified with Histofix® Decalcifier (Panreac, Barcelona, Spain) and dehydrated using graded series of ethanol, and, finally, embedded in paraplast®. Longitudinal sections of 5 μm thick were obtained from each samples with a microtome (Shandon Finesse 325). Sections were stained with hematoxylin-erythrosin for new bone analysis. Bone mineralization was assessed with VOF trichrome staining, in which red and brown tie indicates advanced mineralization, while, less mineralized, newly formed bone stains blue (Martínez-Sanz, et al., 2011). Sections were analyzed through LEICA DM 4000B light microscopy. Computer based image analysis software Leica Q-win V3 Pro-image Analysis System (Barcelona, Spain) was used as a tool to evaluate extracted sections. A region of interest (ROI) within the lesion was delimited (12.5 mm^2) for

quantitative evaluation of new bone formation. The latter was expressed as repair percentage with respect to the original defect area within the ROI.

Regarding immunohistochemical analysis, sections were deparaffined and rehydrated in Tris-buffered saline (TBS) (pH 7.4, 0.01 M Trizma base, 0.04 M Tris hydrochloride, 0.15 M NaCl), which was employed for further incubations and rinse steps. Sections were incubated with citrate buffer (pH 6) at 90 °C for antigen retrieval, afterwards incubated in 0.3% hydrogen peroxide in TBS buffer during 20 min. Posterior to a rinse step, sections were blocked with 2% FBS in TBS–0.2% Triton X-100 (blocking buffer). The indirect immunohistochemical analysis was carried out by incubating sections with osteocalcin (OCN) polyclonal antiserum (1/100) (Millipore, Barcelona, Spain) in blocking buffer overnight, at 4 °C. Sections were washed three times and incubated with biotin-SP-conjugated donkey anti-rabbit F (ab0) fragment (1/500) (Millipore, Barcelona, Spain) using blocking buffer for 1 h followed, after another rinse step, by incubation in peroxidase-conjugated streptavidin (1/500) (Millipore, Barcelona, Spain) for 1 h. Tris–HCl buffer (0.05 M, pH 7.6) containing 0.005% of 3.3′ diaminobencidine (Sigma, Poole, UK) and 0.01% hydrogen peroxide was used to reveal peroxidase activity. The specific antiserum was replaced with normal serum to confirm reaction specificity.

OCN staining was analyzed using ImageJ (NIH, Bethesda, MD) computer-based image analysis software. Measurement of OCN staining was obtained by employing a fixed threshold to select for positive staining within the ROI. Positive pixel areas were divided by the total surface size (mm^2) of the ROI and values were normalized with blank scaffolds and were reported as relative staining intensities.

Neovascularization was determined using blood vessel density and vessel surface area within the ROI. To that aim, sections were labeled with an anti-CD34 monoclonal antibody (1/50) (DAKO, Barcelona, Spain) in blocking buffer, overnight at 4 °C. Sections were washed three times before incubating them with biotin-SP-conjugated donkey anti-rabbit F(ab0) fragment (1/500) (Millipore, Barcelona, Spain) in blocking buffer for 1 h. Afterwards, another rinse step was done and samples were incubated in peroxidase-conjugated streptavidin (1/500) (Millipore, Barcelona, Spain) for 1 h. Tris–HCl buffer (0.05 M, pH 7.6) containing 0.005% of 3.3′ diaminobencidine (Sigma, Poole, UK) and 0.01% hydrogen peroxide was employed to reveal peroxidase activity. Reaction specificity was validated by replacing the specific antiserum with normal serum. Blood vessel density was defined in absolute values and vessel surface area in mm^2 based on the quantitative evaluation of the ROI.

2.13. Statistical analysis

Statistical analysis was realized with SPSS.25 software. Normal distribution of the data was evaluated using Shapiro-Wilk test. For normal distribution of the data, particularly for differences between two groups Studenťs *t*-test was employed, while one-way ANOVA and Tukey as post-hoc test were applied for multiple comparisons. Besides, non-normally distributed data was analyzed with Mann-Whitney nonparametric analysis or Kruskal-Wallis test with Dunńs multiple comparisons tests. P values < 0.05 were considered as significant and illustrated by different symbols. Data are expressed as mean ± standard deviation.

3. Results & discussion

3.1. Fabrication and protein adsorption studies of the 3D scaffolds

In this study, nanoreinforced double-crosslinked 3D scaffolds have been successfully synthetized, characterized and tested for bone tissue engineering purposes. The simple mixing technique was efficiently applied for the biofabrication of combinatorial systems which were compounded of HA and Al in the case of C2 and HA, Al and MMT nanoclay in the case of M2. As seen in Fig. 1a, C2 hydrogels were completely translucent, while M2 hydrogels had some opacity due to the nanoclay, yet both hydrogels showed a homogeneous distribution of cells.

Swelling behaviour, degradation rates, porosity and mechanical properties of C2/M2 scaffolds were studied in a previous work (Hasany, et al., 2018). It has been demonstrated that the wettability of both hydrogels as well as porosity and physiological stability meet the requirements; remarkably, M2 exhibited enhanced mechanical properties. These results confirmed that the systems are able to favor the proper transport of nutrients and oxygen, at the same time mimic the load-

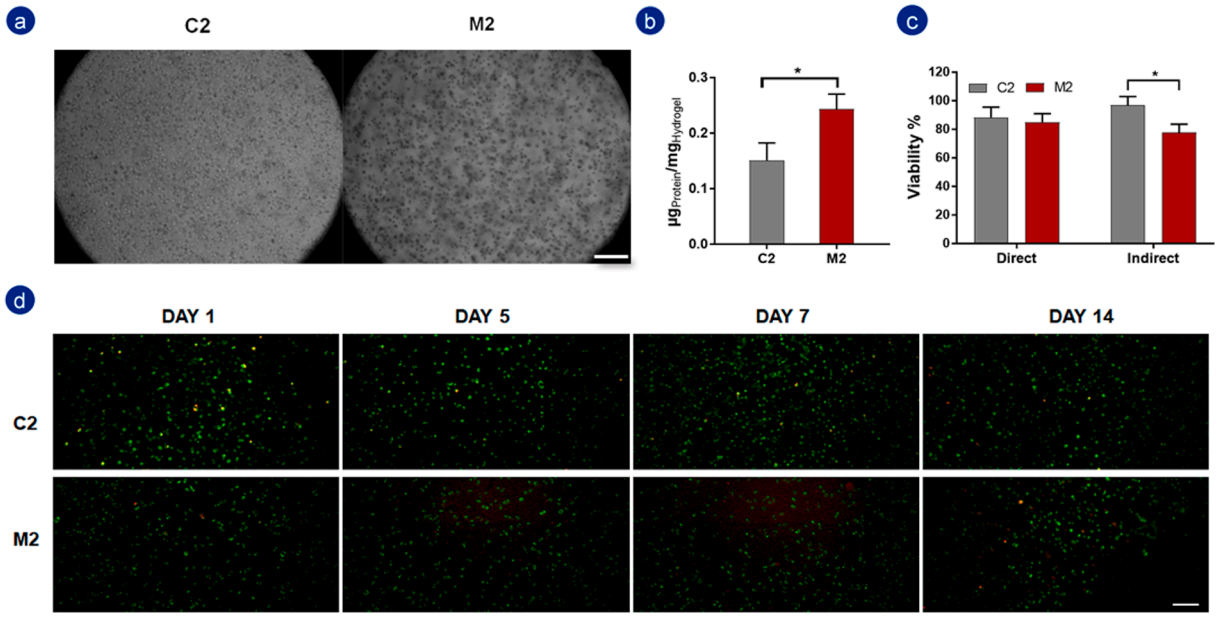

Fig. 1. C2 and M2 hydrogels. (A) Optical images of C2 and M2 embedded with mMSCs after 1 h of fabrication. Scale bar = 175 μm. (B) Protein adsorption study. *p < 0.05 Data represent mean ± standard deviation (n = 5). (C) Biocompatibility assay as described by the guideline ISO 10993, graphs show the viability of mMSCs within C2/M2 scaffolds for both direct contact and the contact with the extracts. *p < 0.05 Data represent mean ± standard deviation (n = 5) (D) Live/Dead assay during 1, 5, 7 and 14 days for both C2 and M2 scaffolds. Scale bar = 100 μm.

bearing environment of the native bone tissue.

To delve into the abilities that these scaffolds may own, a protein absorption study was done. Apart from the correct micro- and nano-architecture, scaffolds used in bone tissue engineering must show proper protein adsorption capacity. Once a tissue engineered construct is implanted, interaction with native media occurs together with the adsorption of proteins (Chang, 2011). The latter may favour cell-scaffold interaction, which can lead to better cell adhesion, survival and proliferation (Bilginer, et al., 2021; Chang, 2011). In this study, M2 scaffold showed an advantageous and significant protein adsorption capacity in contrast to C2 (Fig. 1b), which can be attributed to the electrostatic bonds generated between the MMT and the protein.

3.2. In vitro biocompatibility studies

Amidst all the requirements that tissue-engineered scaffolds must meet, biocompatibility is among the most important ones (Naahidi, et al., 2017; Stamnitz and Klimczak, 2021). Herein, two different studies were used to determine the biocompatibility of the systems. First, direct and indirect cytotoxicity studies were carried out following the guideline ISO 10,993 (Biological evaluation of medical devices guideline: cytotoxicity on extracts and cytotoxicity by direct contact) with L-929 fibroblasts. No cytotoxic effects were seen in the test groups (Fig. 1c), although C2 hydrogels showed more biocompatibility in comparison with M2 when it comes to the extracts. All hydrogels passed the stipulated threshold of 70% viability normalized to control, thus it could be concluded that the bioengineered systems are biocompatible.

Nevertheless, and in order to obtain more information about the issue, a live/dead assay was carried out with mMSCs for 2 weeks (Fig. 1d). Qualitative fluorescent images revealed that most cells remain viable for 14 days, both in C2 and M2 hydrogels, ratifying the proper biocompatibility of all scaffolds and their suitability as tissue-engineered systems. It is certain that the fluorescence intensity decreases over time and this is due to the fact that both scaffolds gradually become more opaque during the culture period.

3.3. ALP and ARED stainings

Once the main characteristics of the scaffolds, as well as their biocompatibility were investigated with promising results, their bioactivity was studied. First, a three-week ALP staining study was carried out to determine whether mMSCs had differentiated to osteoblasts. ALP is an enzyme found in the membrane of osteoblasts and plays a primary role in mineralization. It is considered an early marker of osteogenesis and gives an idea about the differentiation of mMSCs (Noda, 1993). As seen in Fig. 2a/b, an increase in the stained area can be noted with differentiation media in every week. Although the C2 hydrogels show more advantage in the first week, the M2 ones stand out more in the long term (week 2), to end up matching with C2 in the third week, which may lead to conclude that both hydrogels display a similar overall efficacy. Nonetheless, an increase in ALP was marked on the third week even without the differentiation media in both types of hydrogels. The latter may indicate that the scaffolds themselves provide osteogenic properties. For further analysis, ARED staining was performed at week 5. Once the cells are differentiated into osteoblasts, they produce calcium deposits which can be detected by ARED staining (Ghosh, et al., 2019). Optical images showed the increase of calcium depositions during time, especially in the M2 group with differentiation media (Fig. 2c). Once the photos were taken, the absorbed ARED of each sample was extracted and quantified. Fig. 2d indicates that M2 scaffolds with differentiation media showed significantly higher ARED absorption compared to C2/M2 scaffolds with normal media, demonstrating the possible efficacy of M2 scaffolds for bone regeneration.

3.4. Mineralization studies

With the aim of studying the mineralization of the samples after 5 weeks of incubation, SEM, EDAX, FTIR and XRD studies were performed. SEM images showed no mineralization on C2 hydrogels with normal media, while all the other ones –especially M2 with differentiation media- showed clear mineralization structures within the scaffolds (Fig. 3a). To further confirm the data, FTIR and XRD analysis were conducted. From the FTIR results, $\nu_4(PO_4^{3-})$ peak was observed in all

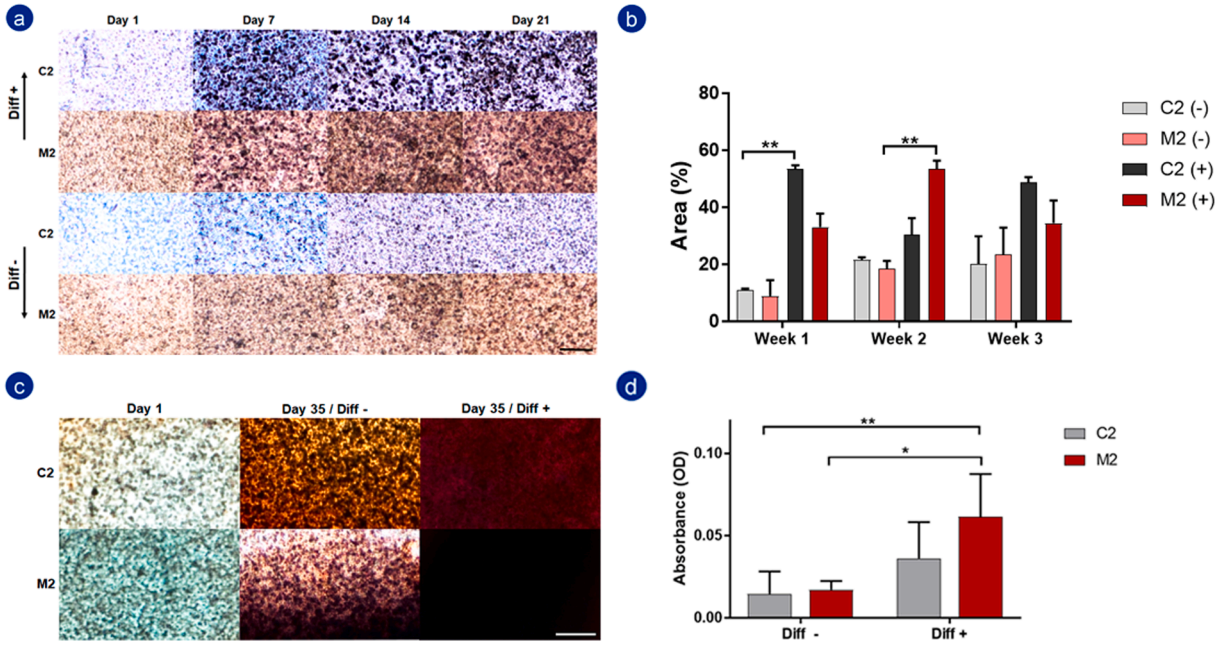

Fig. 2. ALP and ARED stainings. (A) Optical images of scaffolds stained with BTCPT showing intracellular ALP for three weeks, both with normal media (-) and differentiation media (+) Scale bar = 150 μm. (B) Semiquantitative analysis of BTCP stained area of each group. **p < 0.01 (C) Alizarin Red staining after 5 weeks of incubation, both with normal media (Diff -) and differentiation media (Diff +). Scale bar = 150 μm. (D) Quantitative analysis of bonded ARED, displayed as absorbance values. *p < 0.5 **p < 0.01. (For interpretation of the references to colour in this figure legend, the reader is referred to the web version of this article.)

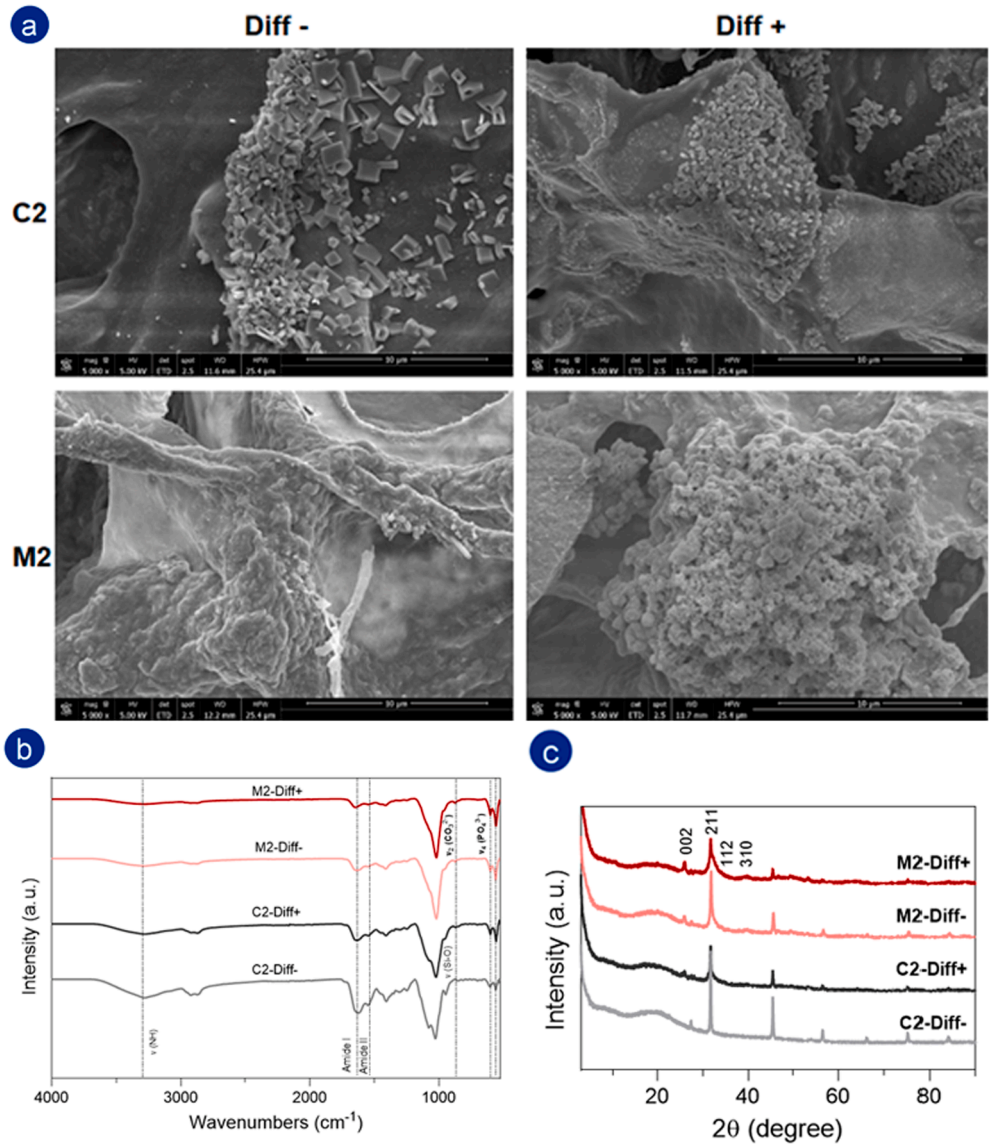

Fig. 3. Mineralization studies. (A) SEM images showing the mineralization of each type of hydrogel in different culture medias (Diff - and Diff +). Scale bar = 10 μm. (B) FTIR spectra and (C) XRD analysis.

samples except in C2 with normal media, which supports the SEM results. Similar outcomes can be deduced from XRD analysis, where two important hydroxyapatite-related peaks (0 0 2) and (2 1 1) were recognized in almost all the samples, except in C2 ones with normal media.

Namely, it can be concluded that few or no mineralization takes place on C2 with normal media, but mineralization occurs when the scaffold came into contact with osteoinductive media. Singularly, M2 scaffolds showed mineralization even without the differentiation media, although the mineralization is greater in samples incubated in differentiation media, which confirms the ability of these structures to enhance mineralization.

In addition to what has been stated, EDAX analysis was performed to investigate the chemical composition of hydrogels (Fig. 4 and Table 2). As in previous studies, with exception of C2 hydrogels in normal media, all the groups showed a Ca/P ratio close to that of hydroxyapatite (2.16) and natural bone (Zaichick and Tzaphlidou, 2003), which confirmed the presence of the minerals. In contrast to ARED staining quantification, EDAX analysis revealed a higher Ca/P ratio in M2 scaffolds even without osteoinductive media, suggesting that those scaffolds themselves –without an inductive environment- could be able to boost osteogenic differentiation and bone mineralization.

On the whole, mineralization studies bring to light the osteogenic ability of M2 scaffolds, which could be attributed to the addition of nanoclay and its already known osteogenic properties (Erezuma, et al., 2021).

3.5. *In vivo studies*

Once the potentiality of scaffolds *in vitro* was confirmed, *in vivo* tests were performed (Fig. 5a). For that purpose, 4 experimental groups were designed for each type of scaffold (C2, M2): empty lesion, blank scaffolds, scaffolds embedded with mMSCs and scaffolds loaded with SDF-1. In this way, we aimed to study the efficacy of scaffolds to regenerate bone as well as their usefulness to act as delivery-platforms for cells or biomolecules such as SDF-1.

Regarding bone repair ability, histological analysis 8 weeks post-implantation showed little repair response in the control group (empty defects) with the presence of bone neoformation in some areas of the margin and some connective tissue occupying a large part of the defect site (Fig. 5a). Animals implanted with blank hydrogels (C2/M2) showed an increase in bone neoformation with respect to the control group. New bone was mainly observed in the periphery of the defect, while the

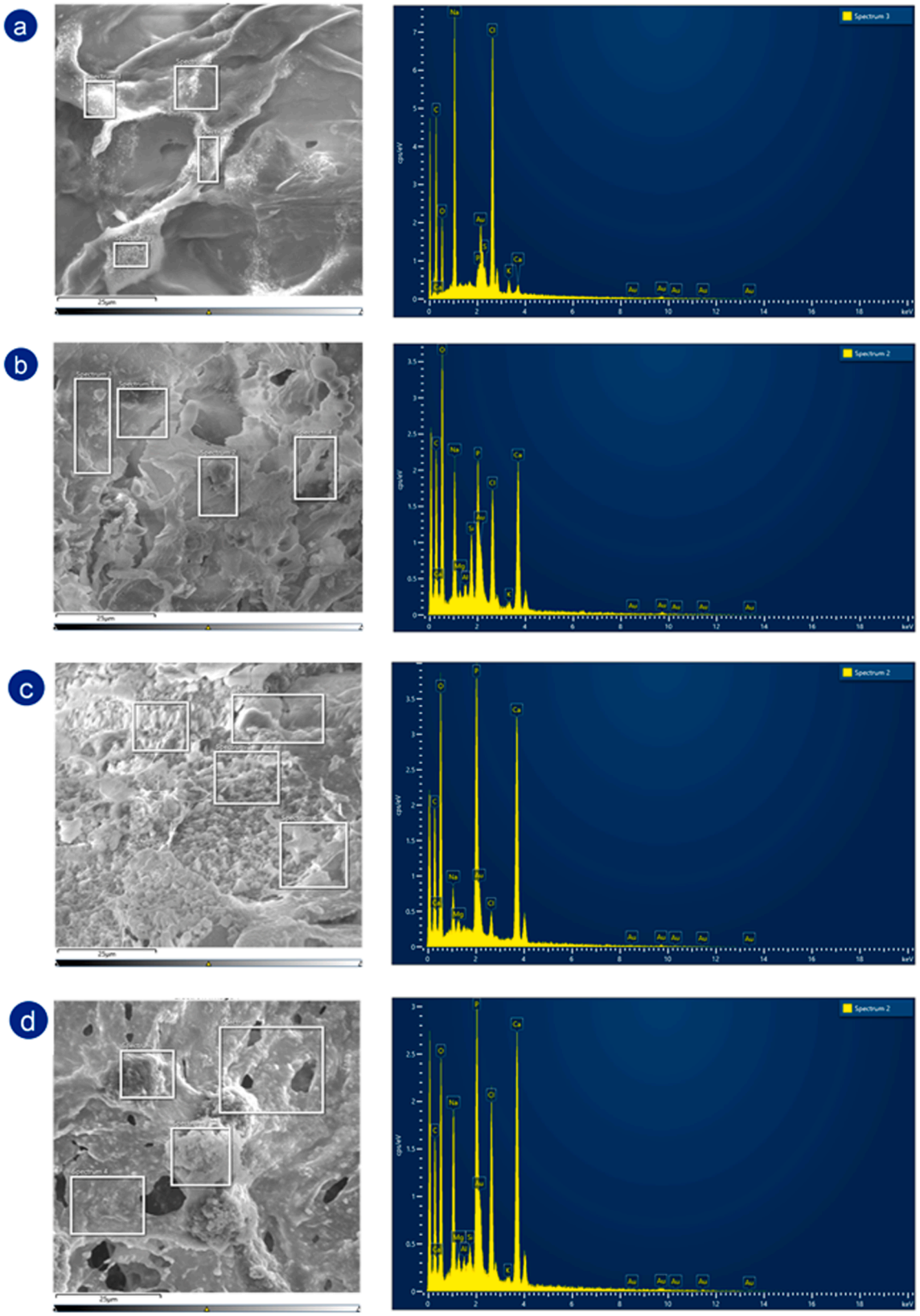

Fig. 4. EDAX analysis of (A) C2 with normal media, (B) M2 with normal media, (C) C2 with differentiation media and (D) M2 with differentiation media.

central area was filled by relative amounts of connective tissue. With scaffolds embedded with cells, slightly better results were obtained (Fig. 5b). Repair percentages for each group was found as follows: 23.4 and 28.8 with C2 hydrogels, and 18.3 and 25.4 with M2 hydrogels, without significant differences between them in each case.

Nevertheless, the repair responses obtained with C2 and M2 hydrogels containing SDF-1 were significantly higher; these groups displayed repair percentages between 42.1 and 36.1 with C2 hydrogel and M2

Table 2
EDAX analysis of different experimental groups after 5 weeks. Ca and P results were showed as weight percentage.

Sample		Ca (%)		P (%)		Ca/P Ratio
		Mean	SD	Mean	SD	
Diff -	C2	0.81	0.21	0.50	0.25	1.62
	M2	7.10	3.06	3.23	1.45	2.20
Diff +	C2	15.88	3.91	8.78	2.01	1.80
	M2	7.99	4.50	3.78	2.35	2.11

hydrogels respectively, and important areas of the defect were filled by neoformed bone with similar histological characteristics to the adjacent host tissue (Fig. 5c), although no statistically significant differences were found between C2 and M2.

The results of the expression of OCN -marker of late osteogenesis and mineralization- in the newly formed bone showed a direct correlation with histological and histomorphometric results, being significantly higher in the groups implanted with hydrogels containing SDF-1, with respect to the control and blank hydrogels (Fig. 6).

Finally, angiogenesis was examined, since it is an essential step for an appropriate bone regeneration. The analysis of vascularization with anti-CD34, a widely used indicator of neovascularization or formation of new blood vessels, revealed a significant increase of vascular parameters, blood vessel density and vessel surface area, in the experimental groups implanted with hydrogels containing SDF-1 and cells, being higher in the SDF-1 group, with respect to the control and blank hydrogels (Fig. 7).

In this study, *in vivo* results did not fully harmonize with those obtained *in vitro*. M2 scaffolds seemed to be more suitable *in vitro*, since MMT conferred improved mechanical characteristics and protein adsorption and mineralization abilities to the hydrogel. Nevertheless, C2 and M2 scaffolds did not obtain statistically significant differences *in vivo*. These results could be explained by several potential reasons. First, it is conceivable that the number of loaded cells in the hydrogels for the *in vivo* experiments was lower than ideal to provide a differential

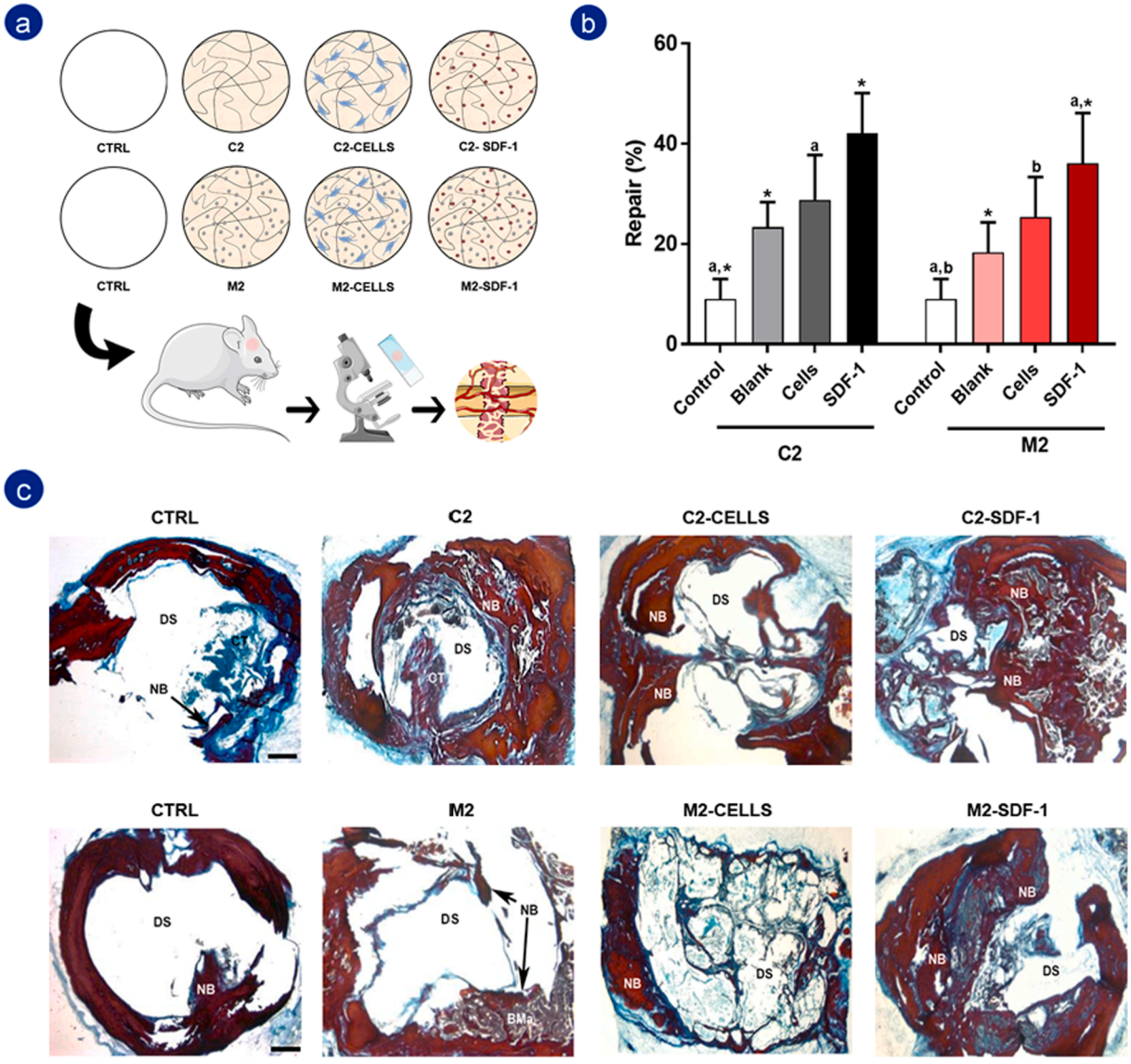

Fig. 5. (A) Schematic illustration about *in vivo* studies. Some representative figures were taken from 'Smart Servier Medical Art' (https://smart.servier.com/). (B) Graph displaying repair percentage of different experimental groups. Histograms represent the mean ± SD. The same letters or symbol on different histograms indicates significant differences between those groups. (C) Representative images in horizontal section with VOF staining technique, showing repair response with both hydrogels (C2 and M2), in the different experimental groups 8 weeks postimplantation. Areas of regenerated new bone (NB) can be observed in all images, as well as the bone microarchitecture. BMa: Bone marrow, CT: Connective tissue, DS: Defect site, NB: Newly formed bone. Scale bars = 500 μm.

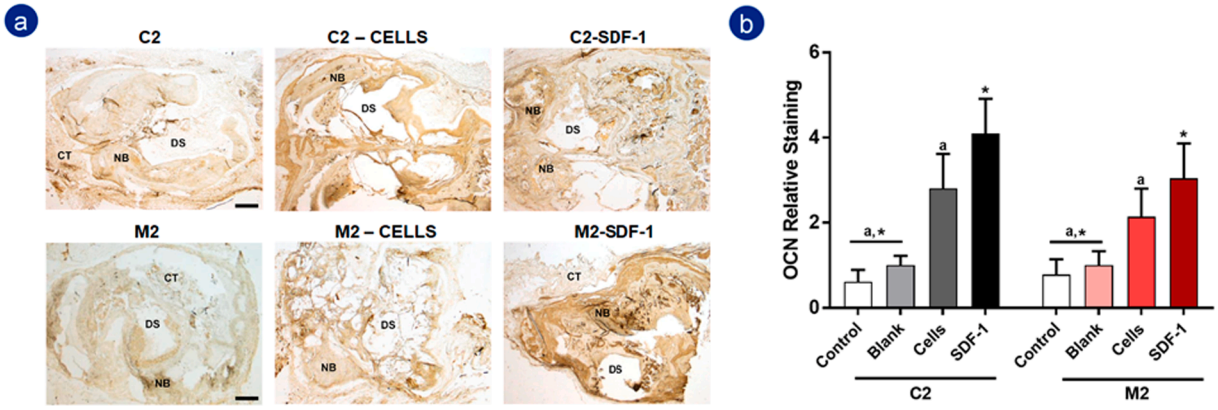

Fig. 6. (A) Representative images in horizontal section showing OCN immunoreactive staining in the defect site, with both hydrogels (C2 and M2), in the different experimental groups 8 weeks postimplantation. (B) The graph shows the OCN relative staining in arbitrary units in the different experimental groups. Histograms represent the mean ± SD. The same letters or symbol on different histograms indicates significant differences between these groups. CT: Connective tissue, DS: Defect site, NB: Newly formed bone. Scale bar = 500 μm.

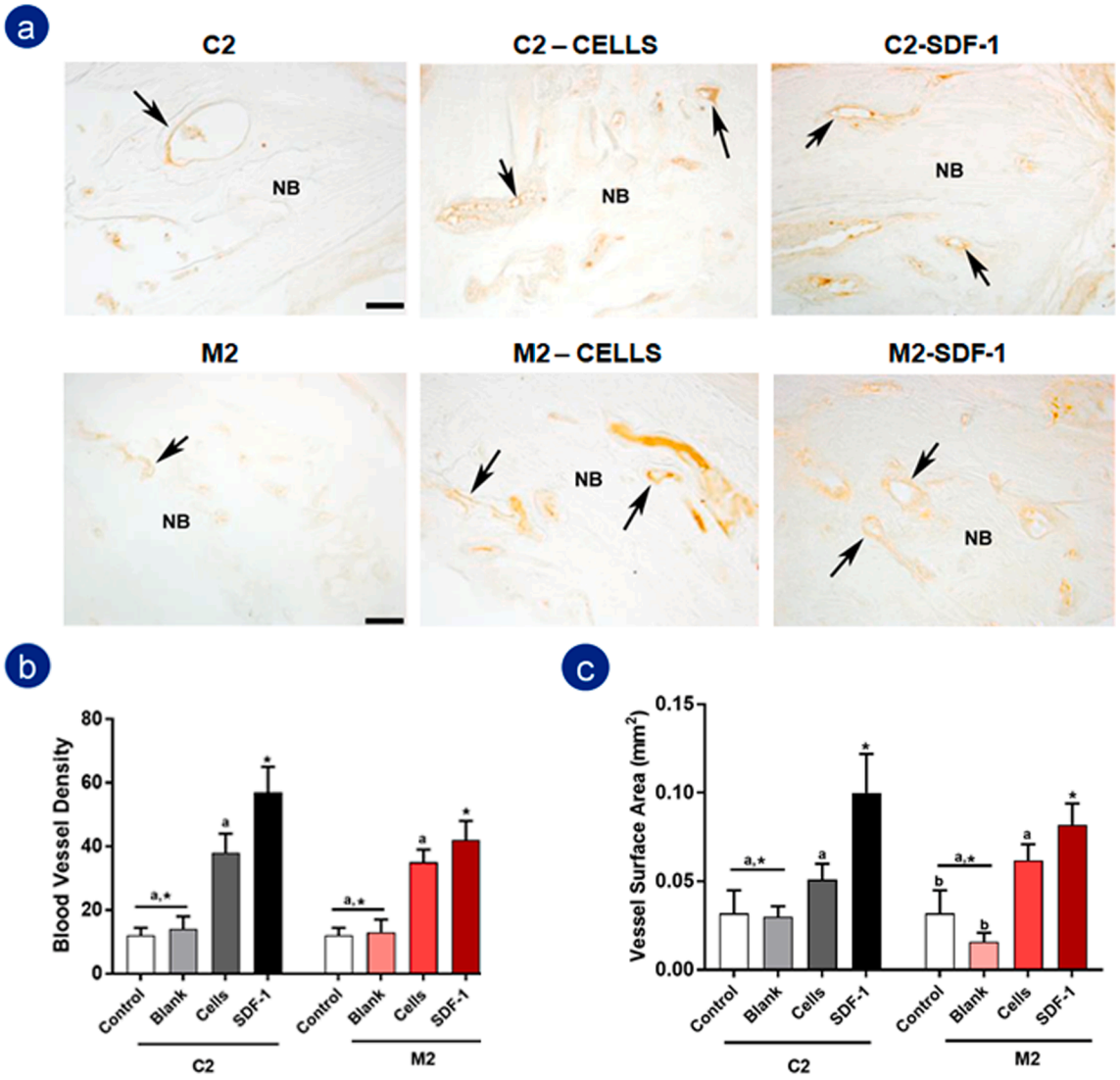

Fig. 7. (A) Representative images in horizontal section showing CD34 immunoreactive staining in the defect site, with both hydrogels (C2 and M2), in different experimental groups 8 weeks postimplantation. The immunoreaction can be seen mainly in the endothelial cells lining the lumen of the blood vessels (arrows). (B) Blood vessel density and (C) vessel surface area (mm^2) within the ROI in the different experimental groups. Histograms represent the mean ± SD. The same letters or symbol on different histograms indicates significant differences between these groups. NB: Newly formed bone. Scale bar = 50 μm.

performance in the case of M2 scaffolds. Second, it is also conceivable that the enhanced mechanical stability of the M2 hydrogels could be better adapted to a more demanded load-bearing animal model, in which differences between C2 and M2 may clearly be more evident. Third, it is unlike but can not be excluded that the dose of nanoclays loaded in the hydrogels could have resulted in toxic effects in the mid term for the enclosed cells. Indeed, there are several studies concerning the potential toxicity of nanoclays (Maisanaba, et al., 2015), and although there are studies approving its biocompatibility, there is still no total certainty about it (Erezuma, et al., 2021). Last but not least, it is necessary to consider that the correlation between *in vitro* and *in vivo* studies carried out with biomaterials is not always ideal (Hulsart-Billström, et al., 2016). Although *in vitro* studies are vital in the search for new treatments, they sometimes face difficulties to mimic the complex native tissues (Bassi, et al., 2021), therefore results can not always be translated.

It is worth noting that *in vivo* studies concluded the usefulness of these hydrogels particularly as SDF-1 delivery-platforms for bone tissue engineering purposes. Furthermore, it has been proven that SDF-1 could be an effective tool when regenerating damaged tissues as it operated as homing factor attracting progenitor cells to the injury site and enabling worthier healing (Bianchi and Mezzapelle, 2020). The direct incorporation of the chemokine into 3D systems –as in the present study- or the overexpression of it on stem cells are fruitful methods to improve bone regeneration (Bianchi and Mezzapelle, 2020; Lau and Wang, 2011; Yang, et al., 2018).

All over, although future studies are needed to provide further insights on cell-carrier potentials, our results provide evidence that HA- and alginate-based scaffolds can be a promising tool in the area of bone tissue engineering.

4. Conclusion

In this study, nanoreinforced hyaluronic acid- and alginate-based scaffolds were successfully fabricated, characterized and tested both *in vitro* and *in vivo*. The simple mixing technique used to create them, and their proved biocompatibility and bioactivity *in vitro,* leave evidence of the potential of these structures for bone tissue engineering. Moreover, *in vivo* studies confirmed their ability to regenerate bone, although no significant differences were seen between the hydrogels with or without the nanoclay. Overall, our results showed the utility and suitability of these scaffolds to act as cell carriers and SDF-1 delivery-platforms for bone tissue regeneration.

CRediT authorship contribution statement

Itsasne Erezuma: Investigation, Formal analysis. **Izeia Lukin:** Investigation, Formal analysis. **Carolina Pimenta-Lopes:** Investigation, Formal analysis. **Francesc Ventura:** Investigation, Formal analysis. **Patricia Garcia-Garcia:** Investigation. **Ricardo Reyes:** Investigation. **M[a] Rosa Arnau:** Investigation. **Araceli Delgado:** Investigation. **Nayere Taebnia:** Investigation. **Firoz Babu Kadumudi:** Investigation. **Alireza Dolatshahi-Pirouz:** Conceptualization, Investigation, Formal analysis. **Gorka Orive:** Conceptualization, Investigation, Formal analysis, Writing – original draft, Visualization.

Declaration of Competing Interest

The authors declare that they have no known competing financial interests or personal relationships that could have appeared to influence the work reported in this paper.

Acknowledgements

This work was supported by the Spanish Ministry of Economy, Industry, and Competitiveness (PID2019-106094RB-I00/AEI/10.13039/501100011033) and technical assistance from the ICTS NANBIOSIS (Drug Formulation Unit, U10) at the University of the Basque Country. We also appreciate the support from the Basque Country Government (Grupos Consolidados, No ref: IT907-16). I. Erezuma and I. Lukin thank to the Basque Government for the PhD grants (PRE_2021_2_0021 & PRE_2021_2_0023). C. Pimenta-Lopes is a recipient of a F.P.U. fellowship from the Ministry of Universidades. A.D.-P. would like to acknowledge the Danish Council for Independent Research (Technology and Production Sciences, 8105–00003B), and the VIDI research programme with project number R0004387, which is (partly) financed by The Netherlands Organisation for Scientific Research (NWO). This work has also received funding from the European Union's Horizon 2020 research and innovation programme under grant agreement No 951747.

References

Amiryaghoubi, N., Fathi, M., Noroozi Pesyan, N., Samiei, M., Barar, J., Omidi, Y., 2020. Bioactive polymeric scaffolds for osteogenicrepair and bone regenerative medicine. 40, 1833-1870.

Bai, X., Gao, M., Syed, S., Zhuang, J., Xu, X., Zhang, X., 2018. Bioactive hydrogels for bone regeneration. Bioact. Mater. 3, 401–417. https://doi.org/10.1016/j.bioactmat.2018.05.006.

Bassi, G., Grimaudo, M.A., Panseri, S., Montesi, M., 2021. Advanced multi-dimensional cellular models as emerging reality to reproduce in vitro the human body complexity. Int. J. Mol. Sci. 22, 1195. https://doi.org/10.3390/ijms22031195.

Bianchi, M.E., Mezzapelle, R., 2020. The chemokine receptor CXCR4 in cell proliferation and tissue regeneration. Front. Immunol. 11, 2109. https://doi.org/10.3389/fimmu.2020.02109.

Bilginer, R., Ozkendir-Inanc, D., Yildiz, U.H., Arslan-Yildiz, A., 2021. Biocomposite scaffolds for 3D cell culture: Propolis enriched polyvinyl alcohol nanofibers favoring cell adhesion. J. Appl. Polym. Sci. 138, 50287. https://doi.org/10.1002/app.50287.

Chang, H., 2011. Cell Responses to Surface and Architecture of Tissue Engineering Scaffolds. In: Anonymous , IntechOpen.

Deo, K.A., Lokhande, G., Gaharwar, A.K., 2015. Nanostructured Hydrogels for Tissue Engineering and Regenerative Medicine, Elsevier Inc.

Dimitriou, R., Jones, E., McGonagle, D., Giannoudis, P.V., 2011. Bone regeneration: current concepts and future directions. BMC Med. 9, 66. https://doi.org/10.1186/1741-7015-9-66.

Echave, M.C., Pimenta-Lopes, C., Pedraz, J.L., Mehrali, M., Dolatshahi-Pirouz, A., Ventura, F., Orive, G., 2019. Enzymatic crosslinked gelatin 3D scaffolds for bone tissue engineering. Int. J. Pharm. 562, 151–161. https://doi.org/10.1016/j.ijpharm.2019.02.043.

Erezuma, I., Eufrasio-da-Silva, T., Golafshan, N., Deo, K., Mishra, Y.K., Castilho, M., Gaharwar, A.K., Leeuwenburgh, S., Dolatshahi-Pirouz, A., Orive, G., 2021. Nanoclay reinforced biomaterials for mending musculoskeletal tissue disorders. Adv. Healthc. Mater. 10, 2100217. https://doi.org/10.1002/adhm.202100217.

Gaharwar, A.K., Cross, L.M., Peak, C.W., Gold, K., Carrow, J.K., Brokesh, A., Singh, K.A., 2019. 2D nanoclay for biomedical applications: regenerative medicine, therapeutic delivery, and additive manufacturing. Adv. Mater. (Weinheim) 31, 1900332. https://doi.org/10.1002/adma.201900332.

Garg, P., Mazur, M.M., Buck, A.C., Wandtke, M.E., Liu, J., Ebraheim, N.A., 2017. Prospective review of mesenchymal stem cells differentiation into osteoblasts. Orthop Surg. 9, 13–19. https://doi.org/10.1111/os.12304.

Ghosh, M., Halperin-Sternfeld, M., Grinberg, I., Adler-Abramovich, L., 2019. Injectable alginate-peptide composite hydrogel as a scaffold for bone tissue regeneration. Nanomaterials (Basel, Switzerland) 9, 497. https://doi.org/10.3390/nano9040497.

Gilbert, W., Bragg, R., Elmansi, A.M., McGee-Lawrence, M.E., Isales, C.M., Hamrick, M. W., Hill, W.D., Fulzele, S., 2019. Stromal cell-derived factor-1 (CXCL12) and its role in bone and muscle biology. Cytokine (Philadelphia, Pa.) 123, 154783. https://doi.org/10.1016/j.cyto.2019.154783.

Hasany, M., Thakur, A., Taebnia, N., Kadumudi, F.B., Shahbazi, M., Pierchala, M.K., Mohanty, S., Orive, G., Andresen, T.L., Foldager, C.B., Yaghmaei, S., Arpanaei, A., Gaharwar, A.K., Mehrali, M., Dolatshahi-Pirouz, A., 2018. Combinatorial screening of nanoclay-reinforced hydrogels: a glimpse of the "Holy Grail" in orthopedic stem cell therapy? ACS Appl. Mater. Interfaces 10, 34924–34941. https://doi.org/10.1021/acsami.8b11436.

Hernández, A., Reyes, R., Sánchez, E., Rodríguez-Évora, M., Delgado, A., Évora, C., 2012. In vivo osteogenic response to different ratios of BMP-2 and VEGF released from a biodegradable porous system. J. Biomed. Mater. Res. A. 100A, 2382–2391. https://doi.org/10.1002/jbm.a.34183.

Hulsart-Billström, G., Dawson, J.I., Hofmann, S., Müller, R., Stoddart, M.J., Alini, M., Redl, H., El Haj, A., Brown, R., Salih, V., Hilborn, J., Larsson, S., Oreffo, R.O.C., 2016. A surprisingly poor correlation between in vitro and in vivo testing of biomaterials for bone regeneration: results of a multicentre analysis. Eur. Cells Mater. 31, 312–322. https://doi.org/10.22203/eCM.v031a20.

Khatoon, N., Chu, M.Q., Zhou, C.H., 2020. Nanoclay-based drug delivery systems and their therapeutic potentials. J. Mater. Chem. B 8, 7335–7351. https://doi.org/10.1039/d0tb01031f.

Lau, T.T., Wang, D., 2011. Stromal cell-derived factor-1 (SDF-1): homing factor for engineered regenerative medicine. Expert Opin. Biol. Ther. 11, 189–197. https://doi.org/10.1517/14712598.2011.546338.

Lee, K.Y., Mooney, D.J., 2001. Hydrogels for tissue engineering. Chem. Rev. 101 (7), 1869–1880.

Maisanaba, S., Pichardo, S., Puerto, M., Gutiérrez-Praena, D., Cameán, A.M., Jos, A., 2015. Toxicological evaluation of clay minerals and derived nanocomposites: a review. Environ. Res. 138, 233–254. https://doi.org/10.1016/j.envres.2014.12.024.

Martínez-Sanz, E., Ossipov, D.A., Hilborn, J., Larsson, S., Jonsson, K.B., Varghese, O.P., 2011. Bone reservoir: Injectable hyaluronic acid hydrogel for minimal invasive bone augmentation. J. Control. Release 152, 232–240. https://doi.org/10.1016/j.jconrel.2011.02.003.

Naahidi, S., Jafari, M., Logan, M., Wang, Y., Yuan, Y., Bae, H., Dixon, B., Chen, P., 2017. Biocompatibility of hydrogel-based scaffolds for tissue engineering applications. Biotechnol. Adv. 35, 530–544. https://doi.org/10.1016/j.biotechadv.2017.05.006.

Noda, M., 1993. Cellular and Molecular Biology of Bone, Acad. Press, San Diego u.a.

Ogay, V., Mun, E.A., Kudaibergen, G., Baidarbekov, M., Kassymbek, K., Zharkinbekov, Z., Saparov, A., 2020. Progress and prospects of polymer-based drug delivery systems for bone tissue regeneration. Polymers 12, 2881. https://doi.org/10.3390/polym12122881.

Rodríguez-Évora, M., Delgado, A., Reyes, R., Hernández-Daranas, A., Soriano, I., San Román, J., Évora, C., 2013. Osteogenic effect of local, long versus short term BMP-2 delivery from a novel SPU–PLGA–βTCP concentric system in a critical size defect in rats. Eur. J. Pharm. Sci. 49, 873–884. https://doi.org/10.1016/j.ejps.2013.06.008.

Salgado, A.J., Coutinho, O.P., Reis, R.L., 2004. Bone tissue engineering: state of the art and future trends. Macromol. Biosci. 4, 743–765. https://doi.org/10.1002/mabi.200400026.

Stamnitz, S., Klimczak, A., 2021. Mesenchymal stem cells, bioactive factors, and scaffolds in bone repair: from research perspectives to clinical practice. Cells (Basel, Switzerland) 10, 1925. https://doi.org/10.3390/cells10081925.

Vacanti, J.P., Atala, A., Langer, R., Lanza, R., 2020. Principles of Tissue Engineering, Academic Press.

Yang, F., Xue, F., Guan, J., Zhang, Z., Yin, J., Kang, Q., 2018. Stromal-Cell-Derived Factor (SDF) 1-Alpha overexpression promotes bone regeneration by osteogenesis and angiogenesis in osteonecrosis of the femoral head. Cell. Physiol. Biochem. 46, 2561–2575. https://doi.org/10.1159/000489684.

Zaichick, V., Tzaphlidou, M., 2003. Calcium and phosphorus concentrations and the calcium/phosphorus ratio in trabecular bone from the femoral neck of healthy humans as determined by neutron activation analysis. Appl. Radiat. Isot. 58, 623–627. https://doi.org/10.1016/S0969-8043(03)00092-7.

Zhang, Y.S., Khademhosseini, A., 2017. Advances in engineering hydrogels. Science (American Association for the Advancement of Science), 356, eaaf3627. doi: 10.1126/science.aaf3627.